

# A device for selecting and rejecting X-ray harmonics in synchrotron radiation beams

Cahit Karanfil,<sup>a\*</sup> Dean Chapman,<sup>b</sup> Carlo U. Segre<sup>a</sup> and Grant Bunker<sup>a</sup>

<sup>a</sup>Physics Division of BCPS Department, Illinois Institute of Technology, Chicago, IL 60616, USA, and <sup>b</sup>Department of Anatomy and Cell Biology, College of Medicine, University of Saskatchewan, Saskatoon, Canada SK S7N 5E5.  
E-mail: karacah@iit.edu

A practical device ('beam cleaner') is described that selects a specific harmonic (e.g. third order) from other nearby harmonics (e.g. fourth or fifth orders) that are transmitted by the beamline monochromator. The ability to isolate and use a clean harmonic beam effectively extends the energy range of existing beamlines. This device is a tunable medium-resolution X-ray bandpass filter, which consists of a double bent Laue crystal post-monochromator. It is a simple and inexpensive device that does not require precision goniometry and can be operated in air. The device can also be used to passively compensate for vertical beam motion as the primary beamline monochromator is scanned. Experimental results are presented that demonstrate the improvement in XAFS data quality under high harmonic conditions.

**Keywords:** X-ray harmonics; XAFS; X-ray monochromators; synchrotron instrumentation; beamlines.

## 1. Introduction

Double-crystal monochromators commonly use low orders of diffraction [e.g. Si(111), Si(220)] to prepare X-ray beams for research at synchrotron sources. These reflections provide high intensity (compared with higher-order reflections) and are adequate for many experiments. However, in some cases it becomes desirable to use the higher-order harmonics from the monochromator to access higher X-ray energies, or alternatively to improve the energy resolution. The use of a higher-order harmonic presents a new problem for the researcher: the selection of that specific harmonic while rejecting the fundamental and other harmonics.

What is needed is a medium-bandwidth optic that would allow the experimenter to select particular harmonics. We have previously shown (Karanfil *et al.*, 2000) that a single bent crystal in Laue geometry can serve this purpose. Here we describe our approach, which uses diffraction from a bent Laue double-crystal system as a moderate bandwidth post-monochromator to select the desired harmonic energy. This crystal system can easily be scanned in energy to track the primary monochromator. Perfect crystals are not ideal in this situation because of their very narrow reflectivity widths. However, the use of highly bent crystals makes the mechanism simpler to construct and align since the crystals provide

a large reflectivity width as well as surprisingly high reflectivity (Erola *et al.*, 1990).

## 2. Bent-crystal optics

Over the past several years bent Laue crystals have been used for a number of applications, including medical imaging (Karanfil *et al.*, 2000; Zhong, 1996; Zhong *et al.*, 1997) and fluorescence EXAFS detection (Karanfil *et al.*, 2000). A surprising aspect of diffraction from an optimized Laue geometry is the high efficiency that such a bent Laue crystal may have, sometimes as high as 80%. A major advantage of a bent-crystal geometry is the enhanced reflectivity width due to the bending of the lattice planes in the transmission geometry. The reflectivity width can be calculated from geometrical and lattice compression considerations to be (Erola *et al.*, 1990)

$$\Delta\theta = \frac{T}{\rho} \left[ \tan(\chi \pm \theta_B) + \frac{1}{2}(1 + \nu) \sin 2\chi \mp \tan \theta_B (\cos^2 \chi - \nu \sin^2 \chi) \right], \quad (1)$$

where  $T$  is the crystal thickness,  $\rho$  is the bending radius,  $\chi$  is the asymmetry angle of the lattice planes with respect to the crystal surface,  $\theta_B$  is the Bragg angle and  $\nu$  is the Poisson ratio for the crystal. Equation (1) gives the expected reflection width of the diffraction that occurs in the crystal. The intensity that is diffracted is more complicated to calculate. For most purposes a kinematic approximation can be made for the diffracted intensity. We will assume that the crystal is bent sufficiently for the crystal to behave as a fully mosaic crystal. In this case the integrated intensity is that given by the kinematic theory and is assumed to be uniform in intensity over the reflectivity width (Zachariasen, 1967).

## 3. Gap and offset determination of the monochromator and a double bent crystal system

The 'beam cleaner' is a double-crystal device that has two bent crystals in Laue geometry with a gap between them set appropriately (Fig. 1). A single crystal is inconvenient to use as a cleaner of the incident beam because the experimental apparatus must follow the diffracted beam if the energy is changed. It can be shown that the

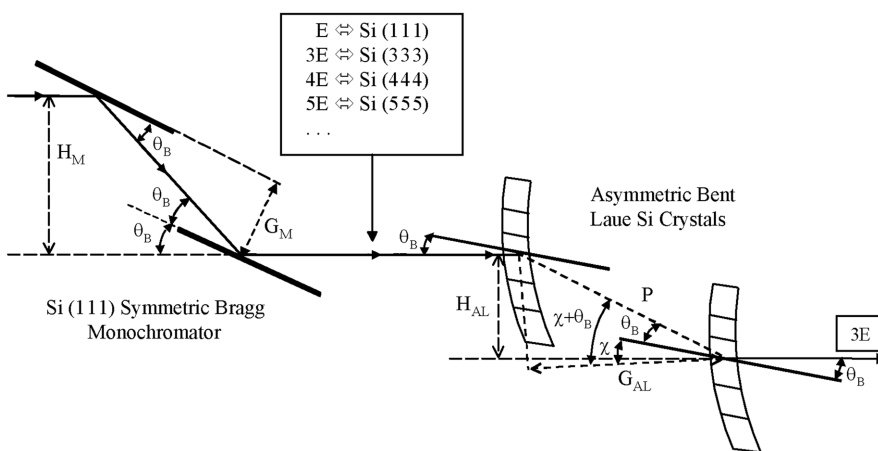


**Figure 1**

Crystal arrangement for the combination of the double-crystal monochromator and double-crystal beam cleaner. The monochromator is assumed to be Si(111) with the harmonics arising from higher-order reflections. The cleaner picks out one of these harmonics using the Si(111); the  $3\times$  fundamental energy is shown as being selected. The upper sign case of diffraction is shown for the cleaner on the incident beam side of the first crystal as described in the text.

variation of the double-crystal beam offset of the Laue-case system is in the opposite sense to the double-crystal Bragg system. For example, in terms of the perpendicular crystal separation  $G_M$  and the offset  $H_M$  of a double-crystal symmetric monochromator in the Bragg case,

$$H_M = 2G_M \cos \theta_M. \quad (2)$$

When the monochromator is rotated about an axis passing through the diffraction surface of the first crystal, the variation in the offset is given by

$$\frac{dH_M}{d\theta_M} = -2G_M \sin \theta_M. \quad (3)$$

Similarly, for the symmetric Laue (SL) case the offset  $H_{SL}$  and variation are

$$H_{SL} = 2G_{SL} \sin \theta_{SL}. \quad (4)$$

Again, for a rotation axis passing through the diffracting region of the first Laue crystal, the variation in the offset is

$$\frac{dH_{SL}}{d\theta_{SL}} = 2G_{SL} \cos \theta_{SL}. \quad (5)$$

Since the offset change for the Bragg case (monochromator) is opposite to that for the Laue cleaner the variation in offset can be removed at an energy. For simplicity, it is assumed that the same reflection is used ( $\theta_M = \theta_{SL} = \theta_B$ ) with a given gap for the cleaner. The combined variation in offset of a tandem monochromator and cleaner system is then

$$\Delta H \cong \frac{dH_M}{d\theta_M} \Delta\theta_M + \frac{dH_{SL}}{d\theta_{SL}} \Delta\theta_{SL}. \quad (6)$$

Since the angle change of each crystal system is the same for a matched crystal system, then

$$\Delta H \cong \left( \frac{dH_M}{d\theta_M} + \frac{dH_{SL}}{d\theta_{SL}} \right) \Delta\theta_{SL}. \quad (7)$$

Therefore the overall offset variation can be removed around the design energy if

$$\frac{dH_M}{d\theta_M} = -\frac{dH_{SL}}{d\theta_{SL}}. \quad (8)$$

This condition gives

$$\frac{G_{SL}}{G_M} = \frac{\sin \theta_B}{\cos \theta_B} = \tan \theta_B. \quad (9)$$

This relationship can be used to define the Laue crystal separation  $G_{SL}$  for a given monochromator gap  $G_M$ . Similar equations for the offset and variation can be derived for the asymmetric Laue (AL) geometry. The asymmetry angle of the lattice planes is  $\chi$  and is measured from the normal direction,

$$H_{AL} = \frac{\sin 2\theta_B}{\cos(\chi \mp \theta_B)} G_{AL} \quad (10)$$

and

$$\frac{dH_{AL}}{d\theta_B} = \left[ \frac{2 \cos 2\theta_B}{\cos(\chi \mp \theta_B)} \mp \frac{\sin 2\theta_B \sin(\chi \mp \theta_B)}{\cos^2(\chi \mp \theta_B)} \right] G_{AL}. \quad (11)$$

Here the upper and lower signs refer to the side of the lattice planes used in relation to the bending radius of the crystal. The upper sign refers to the geometry when the source and bending radius are on the same side of the diffraction planes.

The ratio of crystal separations of the monochromator and cleaner can be found as

$$\frac{G_M}{G_{AL}} = \frac{1}{2 \sin \theta_M} \left[ \frac{2 \cos 2\theta_B}{\cos(\chi \mp \theta_B)} \mp \frac{\sin 2\theta_B \sin(\chi \mp \theta_B)}{\cos^2(\chi \mp \theta_B)} \right]. \quad (12)$$

Thus the possibility of having the beamline monochromator operate in ‘channel cut’ mode in tandem with the cleaner can result in a cleaned beam with no or very little offset variation. Note that these equations assume that the crystals are parallel. This is the only practical crystal arrangement that allows the crystals to be placed in close proximity. These arrangements are  $\chi + \theta_B$  on the first crystal and  $\chi - \theta_B$  on the second crystal or *vice versa*. Arrangements of  $\chi + \theta_B$  (or  $\chi - \theta_B$ ) incident on both crystals result in the crystals intercepting each other for reasonable values of  $\chi$  and crystal size, and these configurations are not considered in this work.

#### 4. Experimental set-up and results

Experiments were performed at the MR-CAT (sector 10) beamline at the Advanced Photon Source at Argonne National Laboratory. The beamline monochromator was a Si(111) double-crystal mechanism. No mirror or post-monochromator optical elements were in place to affect the harmonic spectra.

##### 4.1. Reflectivity measurements

Reflectivity measurements were performed at a number of energies. Results at 18 keV will be shown and are representative of those obtained at other energies. At 18 keV the beamline monochromator was set at 6 keV from the Si(111) and thus Si(333) passed 18 keV. The undulator was set with the fundamental also at 6 keV and the 18 keV harmonic was used as well.

Both crystals of the device were mounted on a common plate. This plate can be rotated to change the energy using a rotary stage (Huber 410). The first crystal was mounted on the rotation axis of the stage. The second crystal was mounted on a translation stage to adjust the perpendicular distance between the crystals (gap). The second crystal also has a rotation adjustment using a second translation stage to move a tangent bar. Both crystals have adjustable bending radii using a screw assembly with spring.

Two argon-filled ion chambers were used to measure the diffracted and transmitted beams from the first and second crystals. The direct beam was blocked downstream of the cleaner assembly by a lead stop. One of the ion chambers was positioned to intercept the diffracted beam from the first crystal passed through the second crystal. The second ion chamber intercepted the beam diffracted by the second crystal. This chamber is used to set the first cleaner crystal to the Bragg angle. This beam is the one to be used in the beam cleaner experiment. The plot in Fig. 2 shows a comparison between the calculated and the measured rocking curve of a pair of 200  $\mu\text{m}$ -thick Si crystals at 18 keV. The measured data are shown as the solid curve. A calculated rocking curve for the two-crystal cleaner is shown as the dashed curve for comparison. This calculation is based on the convolution of the calculated plane-wave rocking curve for each crystal using the *REFLECT* computer code (Eteläniemi *et al.*, 1989). The measured diffraction efficiency of the double bent crystal arrangement is about 45%. The measurements at the other energies (15, 20, 25, 30 keV) with different bending radii are also consistent with those obtained by the *REFLECT* computer program (Figs. 3, 4 and 5).

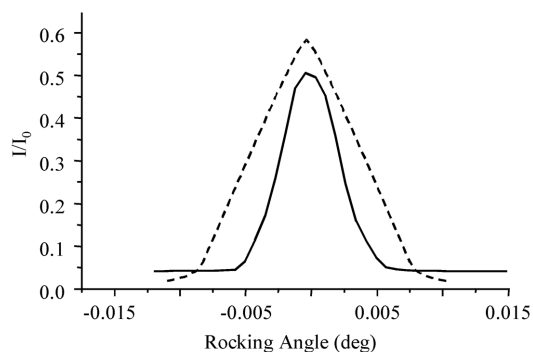


**Figure 2** Reflectivity of the double-crystal beam cleaner at 18 keV. The solid line is from measured data. The dashed line is from calculations made using the *REFLECT* computer program. (The plane-wave reflectivity output of *REFLECT* is convolved with itself to obtain the curve which matches the experimental arrangement of two crystals: one fixed, one rotated in angle.)

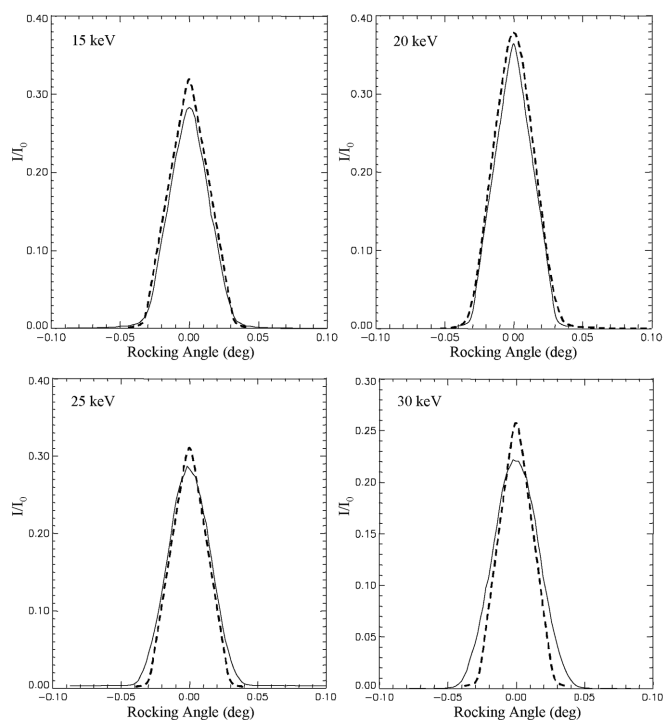


**Figure 3** Reflectivity measurements with 0.7 m bending radius and 15, 20, 25, 30 keV energy. Plots with dashed lines were calculated using the *REFLECT* computer program.

#### 4.2. Offset measurements

To operate the cleaner in tandem with a beamline monochromator, beam motion effects can be eliminated in both devices by using the correct gap between the cleaner crystals [see equations (10) and (12)]. The beamline monochromator offset is 35 mm. The calculated gap required for the beam cleaner to correct for the vertical beam motion in the monochromator fixed-gap mode is 4.5 mm at 19.5 keV. In this case the (333) reflection of the monochromator is selected by the cleaner (111). To confirm the dependence of the offset as a function of gap at a given monochromator energy, the crystal gap was chosen to be large enough for the beam displacements to be easily measurable. Fig. 6 shows the measurements of gap and offset for an energy of 18 keV. There is good agreement between measured and calculated values within the estimated error of the gap–offset measurements.

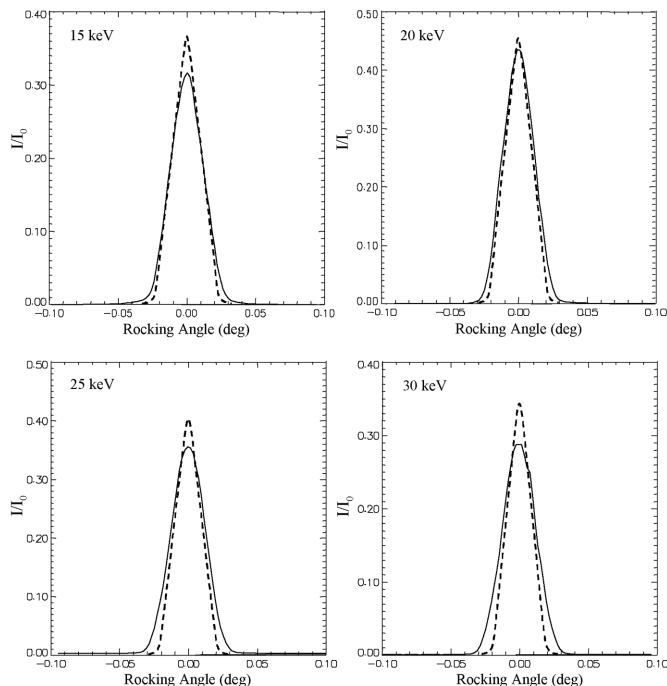


**Figure 4** Reflectivity measurements with 1.0 m bending radius and 15, 20, 25, 30 keV energy. Plots with dashed lines were calculated using the *REFLECT* computer program.

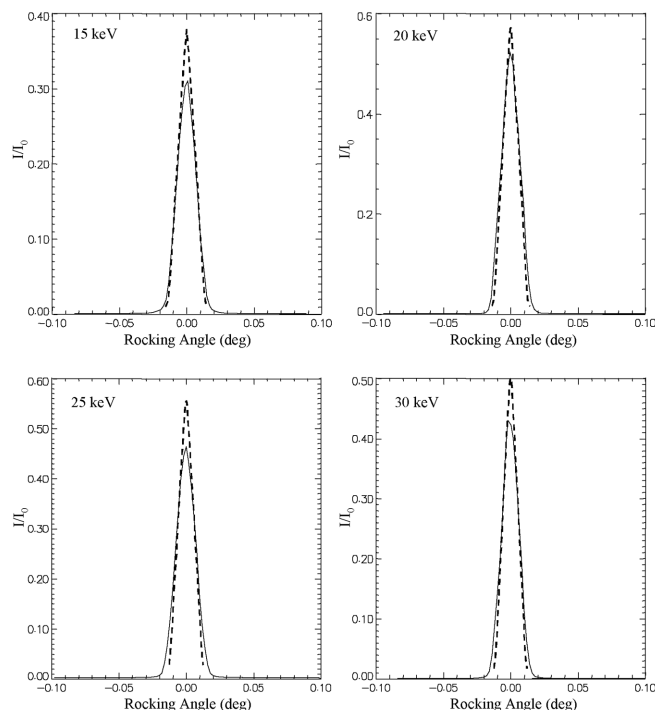


**Figure 5** Reflectivity measurements with 1.7 m bending radius and 15, 20, 25, 30 keV energy. Plots with dashed lines were calculated using the *REFLECT* computer program.

#### 4.3. XAFS measurements with the beam cleaner

Spectral purity of the X-ray beam is essential for accurate X-ray absorption spectra. If harmonics are present, noise is increased

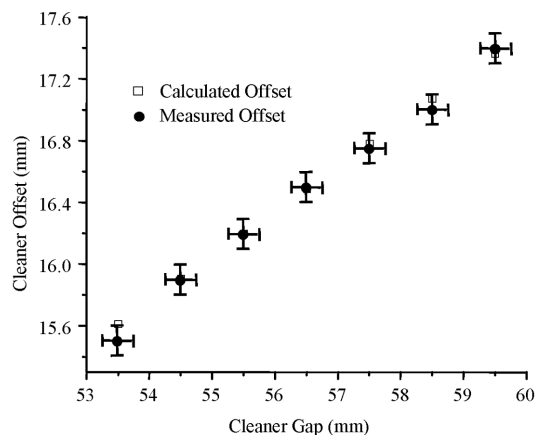


**Figure 6** Gap offset of the beam cleaner at 18 keV. Calculated values are shown as open squares and the measured data with estimated errors (estimated at 250  $\mu\text{m}$  in offset and gap) are shown as solid circles.

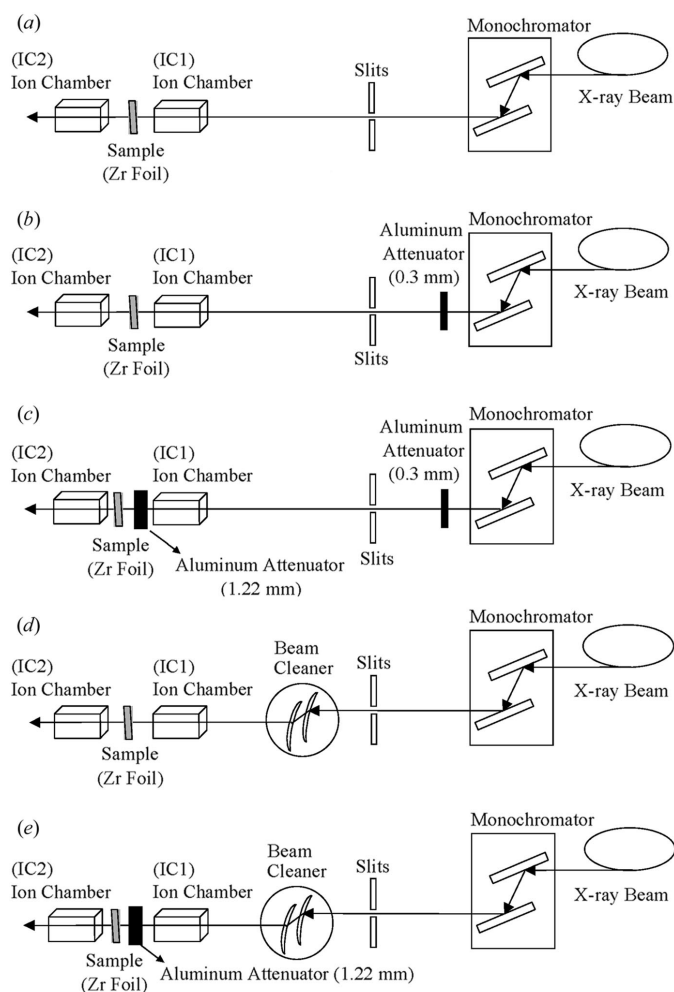


**Figure 7** Experimental XAFS arrangements for testing the performance of the beam cleaner selecting the second harmonic ( $3\times$  fundamental). (a) Reference arrangement, (b) includes an aluminium filter to select the harmonic by blocking the fundamental, (c) includes a thick aluminium attenuator to simulate a thick sample, (d) shows the beam cleaner selecting the second harmonic [to be compared with the arrangement in (b)], and (e) shows the cleaner with the aluminium attenuator [to be compared with the arrangement in (c)].

because variations in intensity of the X-ray beam do not divide out properly in the ratio of detector signals, and spectra are distorted. This effect is especially noticeable in transmission mode because of ‘thickness effects’ (Koningsberger & Prins, 1988; Parrat *et al.*, 1957; Stern & Kim, 1981).

We have previously established the feasibility of selecting harmonics with a single-crystal beam cleaner (Karanfil *et al.*, 2000). In that paper the efficiency of a single-crystal beam cleaner was approximately 70%. In Fig. 3 of that paper the energy spectrum clearly showed that only the desired energy harmonic was transmitted.

In order to demonstrate the ability of a double beam cleaner to reject X-rays at undesired energies during an energy scan, we carried out transmission XAFS measurements on a zirconium foil ( $K$  edge, 17.998 keV) using the Si(333) reflection of the beamline monochromator, the undulator third harmonic and Si(111) reflection of the beam cleaner. The beam cleaner angle was scanned in tandem with the primary monochromator in much the same way that undulator gaps are scanned. Tracking is straightforward because of the relatively large energy bandwidth of the beam cleaner ( $\sim 50$  eV). The monochromator was set to 6 keV (fundamental) for the first XAFS configuration and the (333) reflection of 18 keV was used (Fig. 7a). The XAFS spectrum for this case is shown in Fig. 8.

It is useful to consider the effect of harmonics on the signal-to-noise ratio in transmission XAFS. If no undesired harmonics are present, the absorption coefficient would be given by  $\mu x = \ln(I_0/I_1)$ , where  $I_0$  and  $I_1$  are the intensities measured in detectors placed before and after the sample. In the presence of undesired harmonics,  $h_0$  and  $h_1$  are measured in the two detectors, and the measured absorption coefficient is given by  $(\mu x)_{\text{meas}} = \ln[(I_0 + h_0)/(I_1 + h_1)]$ . However, if the harmonic contamination is small compared with the signal, a first-order expansion gives the error in the absorption coefficient as  $\Delta(\mu x) = (h_0/I_0) - (h_1/I_1)$ . Each of the signals  $I_0$ ,  $I_1$ ,  $h_0$  and  $h_1$  fluctuate in time, but  $I_0$  and  $I_1$  are statistically highly correlated with each other, as are  $h_0$  and  $h_1$ . Note that, even if the harmonic contamination were constant, the fluctuations in  $I_0$  and  $I_1$  generally do not cancel out because the fraction of harmonic contamination will generally be different in the front and rear detectors. The implication is that the error in the absorption coefficient is of the same order of magnitude as the ratio of the harmonic content to the total signal. The variation in absorption coefficient owing to XAFS is typically of the order of several percent. So harmonic contamination

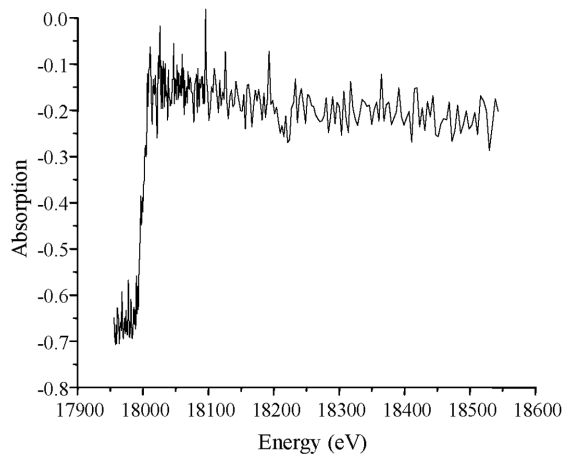


**Figure 8** XAFS spectrum of Zr foil using the Si(333) reflection of the monochromator and third harmonic of the undulator without attenuator and beam cleaner. The experimental set-up for this spectrum is shown in Fig. 7(a).

of the order of a few percent in the beam can completely obscure the EXAFS. This effect is seen in Fig. 8. In addition, the absorption-edge jumps are reduced. Consider a simple calculation of the edge jump under conditions in which the harmonic content ( $h_0$  and  $h_1$ ) are both 10% of  $I_0$ . If the product of the sample thickness and the absorption coefficient increases from 1.0 to 2.0 over the absorption edge (an edge jump of 1.0), the apparent edge jump in the presence of harmonics would be reduced to 0.69, a 31% reduction.

In a real experiment the fundamental would be filtered out in order to reduce contamination from 6 keV. Therefore an aluminium attenuator of thickness 0.3 mm is placed in front of the slits (Fig. 7*b*) to block almost all of the fundamental energy (6 keV) but to transmit 18 keV (70%). The XAFS spectrum for this case is shown in Fig. 9(*a*). As seen in Fig. 9(*a*), the spectrum of Zr foil without the beam cleaner is severely distorted and noisy with a greatly reduced measured edge step. The edge step is substantially reduced from its true value of 17.998 keV, and it is very noisy because fluctuations in measured incident-beam intensity do not divide out correctly. With the beam cleaner (Fig. 7*d*), the spectrum is excellent (Fig. 9*b*).

In order to simulate a thick sample (to further exacerbate thickness effects) we placed a 1.22 mm-thick aluminium attenuator over the sample surface (Figs. 7*c* and 7*e*). This attenuator has the primary effect of 'hardening' the beam, *i.e.* increasing the proportion of high-energy harmonics in the transmitted beam, thereby distorting the

spectra further. Fig. 10 shows the benefit of using the beam cleaner. Without the beam cleaner (Fig. 10*a*) the spectrum of the Zr foil plus 1.22 mm aluminium is even worse, as expected because of the beam hardening effect of the aluminium, *i.e.* the proportion of harmonics in the transmitted beam is increased by the absorption of the aluminium. Even in this extreme case, the beam cleaner produces an excellent spectrum, which is the same as the original spectrum but shifted upward by the aluminium absorption (Fig. 10*b*). They differ only by the additive absorption of the aluminium.

The edge steps and EXAFS amplitudes are not affected by adding the aluminium, as can be seen in Fig. 11 [background-subtracted EXAFS, Fig. 11(*a*), and Fourier transform (FT), Fig. 11(*b*)]. These clearly show no differences between the spectra of the sample with the aluminium and without it. This demonstrates that there is no amplitude reduction due to beam hardening; the beam cleaner effectively removes the harmonic contamination.

### 5. Conclusion

The beam cleaner has been shown to be an effective medium-resolution bandpass monochromator that can be used to select a harmonic from a beamline monochromator. It can improve data

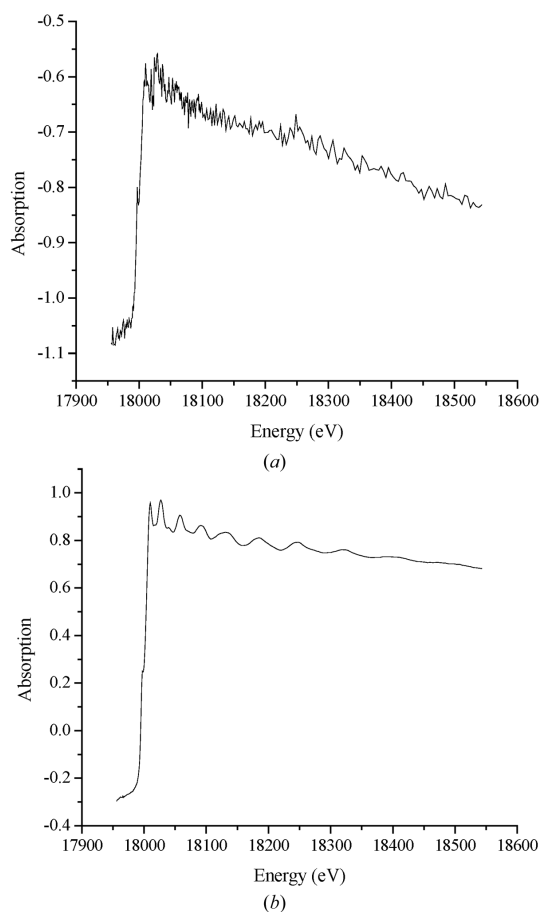


**Figure 9**  
Comparison of XAFS spectra of Zr foil without attenuator using the Si(333) reflection of the monochromator and the third harmonic of the undulator (*a*) without and (*b*) with the beam cleaner. Experimental configurations for these spectra are shown in Figs. 7(*b*) (the fundamental is filtered out by a 0.3 mm-thick aluminium foil in front of the first detector) and 7(*d*).

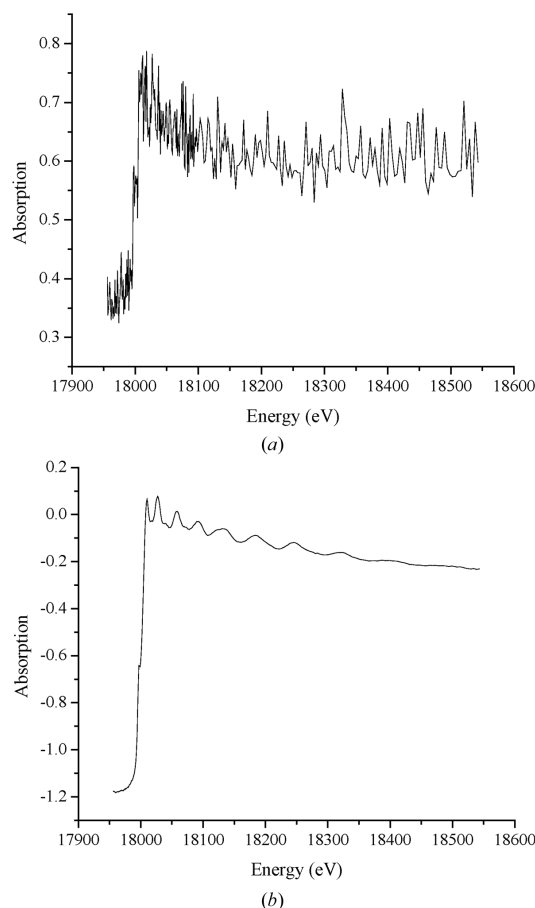


**Figure 10**  
Comparison of XAFS spectra of Zr foil as in Fig. 9 but with an added aluminium attenuator (1.22 mm) on the surface of the sample. The Si(333) reflection of the monochromator and third harmonic of the undulator were used (*a*) without and (*b*) with the beam cleaner. Note that the spectrum in (*b*) is identical to that of Fig. 9(*b*) apart from a vertical shift due to aluminium absorption. Experimental configurations for these spectra are shown in Figs. 7(*c*) and 7(*e*).

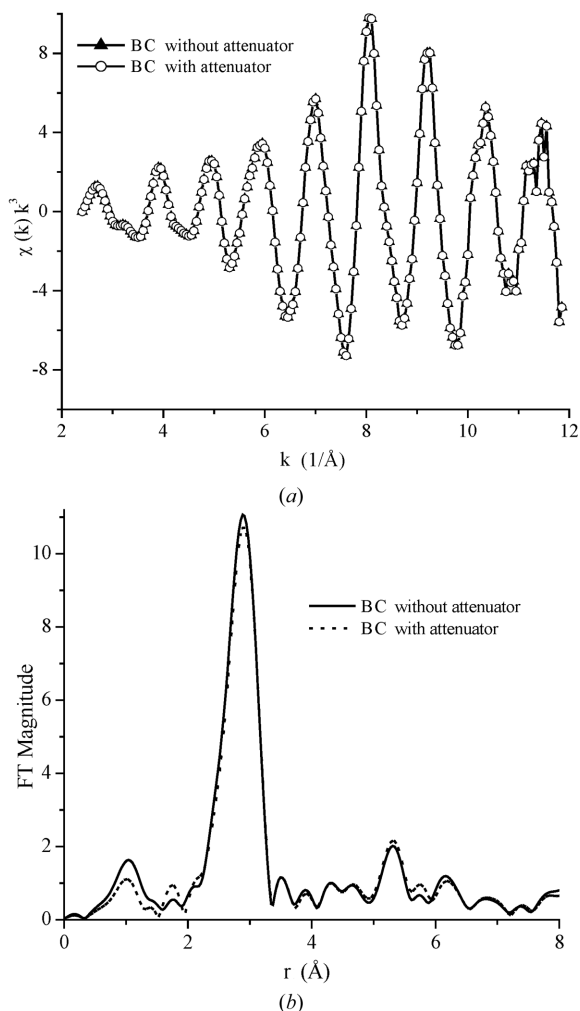


**Figure 11**  
 Comparison of  $k^3$ -weighted EXAFS of Zr foil with and without the aluminium attenuator. The beam cleaner (BC) was used for both cases.

quality by eliminating undesired energies in the beam. A useful feature is that it can be operated in a mode that compensates for beam height changes from the primary monochromator when oper-

ated in channel-cut mode. In many applications a very simple water or liquid-nitrogen-cooled channel-cut monochromator could be used on a beamline provided it was followed by an appropriate beam cleaner.

Beam cleaners can extend the effective energy range of monochromators by making high-order reflections of the primary monochromator more useful, eliminating the need to change crystals to reach high energies. Bent Laue crystals have wide reflectivity curves (and high reflectivity), which allows easy alignment and scanning.

The authors wish to acknowledge useful discussions regarding the device with Zhong Zhong. In addition, the authors would like to thank Thomas Gog and Jeremy Kropf for the loan of some of the equipment used in this experiment. The assistance of Nadia Leyarovska is also gratefully acknowledged. Work performed at MRCAT was supported in part by funding from the Department of Energy under grant number DEFG0200ER45811. We wish to acknowledge the support in part by US Army grant DAMD17-99-1-9217, US DOE contract DE-AC02-CH10886, State of Illinois Higher Education Cooperative Agreement, National Institutes of Health RR08630 and R43 RR018635-01.

**References**

Erola, E., Eteläniemi, V., Suortti, P., Pattison, P. & Thomlinson, W. (1990). *J. Appl. Cryst.* **23**, 35–45.  
 Eteläniemi, V., Suortti, P. & Thomlinson, W. (1989). Report BNL-43247. National Synchrotron Light Source, Brookhaven National Laboratory, Upton, NY, USA.  
 Karanfil, C., Chapman, L. D., Bunker, G. B., Segre, C. U. & Leyarovska, N. E. (2000). *AIP Conf. Proc.* **521**, 276–282.  
 Karanfil, C., Zhong, Z., Chapman, L. D., Fischetti, R., Bunker, G. B., Segre, C. U. & Bunker, B. A. (2000). *AIP Conf. Proc.* **521**, 178–182.  
 Koningsberger, D. C. & Prins, R. (1988). *X-ray Absorption: Principles, Applications, Techniques of EXAFS, SEXAFS and XAFS*. New York: Wiley.  
 Parrat, L. G., Hempsted, C. F. & Jossem, E. L. (1957). *Phys. Rev.* **105**, 1228–1232.  
 Stern, E. A. & Kim, K. (1981). *Phys. Rev. B*, **23**, 3781–3787.  
 Zachariasen, W. H. (1967). *Theory of X-ray Diffraction in Crystals*. New York: Dover.  
 Zhong, Z. (1996). PhD thesis, SUNY at Stony Brook, USA.  
 Zhong, Z., Chapman, D., Menk, R., Richardson, J., Theophanis, S. & Thomlinson, W. (1997). *Phys. Med. Biol.* **42**, 1751–1762.